Self-oscillating polymer membranes with chemically fueled pore size oscillation mediated by pH-responsive polymer

Johanne Pirkin-Benameur, Denis Bouyer, Damien Quemener

Self-oscillating polymer membranes with chemically fueled pore size oscillation mediated by pH-responsive polymer

Johanne Pirkin-Benameur, Denis Bouyer, Damien Quemener*

Institut Européen des Membranes, IEM-UMR 5635, Univ Montpellier, ENSCM, CNRS,34090 Montpellier, France.

*Corresponding author

Email address: damien.quemener@umontpellier.fr (D. Quémener)

Abstract

Soft-matter materials research has considerably evolved in the last decades, mainly by promoting responsive polymer systems. Up to now, the dynamic behavior in materials was always reached by the action of an outside trigger (pH, light, etc..). This constraint has been relieved in a new class of materials that experienced self-oscillation. In this work, the self-regulating pH cycles caused by a chemical oscillator will induce autonomous pH-sensible polymer chain movements at the membrane interface, causing continuous pore-size oscillation cycles and thus a self-oscillating flux. This work involved the functionalisation of polyethersulfone commercial membranes to achieve pore size oscillations. The pH-sensitive polymer, poly(methacrylic acid) (PMAA), was obtained by deprotection of poly(tert-butyl methacrylate) (PtBuMA) synthesized by RAFT polymerization. To adapt this functionalisation to all types of commercial membranes, a thin layer of polydopamine (PDA) was deposited on the top of the membrane, which then allows a Michael-thiol-ene reaction between PDA and thiol-functionalised PMAA, obtained from prior aminolysis of PtBuMA. The functionalisation steps were characterized by XPS, SEM, water contact angle, and permeability measurements. Membranes were then placed in a filtration system containing a chemical pH oscillator to control the PMAA chain conformation through the pH cycle. Water permeation analysis showed a dependence between permeability and PMAA conformation, leading to the conclusion that there is indeed a continuous oscillation in membrane pore size.

Keywords

Self-oscillating membrane; pH oscillator; stimuli-responsive membrane; polydopamine; pH-sensitive polymer

1. Introduction

Our century is filled with many issues, such as chemical pollution [1], which is partly caused by the lack of responsiveness of current materials. This problem and resource shortages are forcing us to develop materials with an improved lifespan, notably through new functionalities. Nature creates materials that meet this challenge, because of their advanced compositions and functions. Thus, one of the major challenges in the materials field is to reach the autonomy level of natural materials. Nowadays materials explored to mimic the nature include stimuli-sensitive systems [2]. Several stimuli have been studied to that purpose such as temperature [3], pH [4], mechanical strength [5], biological triggers [6], and electromagnetic fields [7] for applications such as chromatography [8], surface functionalisation [9], and sensor [10]. pH being one of the most common variables for biological reactions[11,12], pH sensitive polymers have found various applications, especially in biomedical field [13]. pH-sensitive membranes have also been developed due to the potential brought by this trigger such as stimuli-responsive permeation [14], pore size change [15,16], nanoparticle fractionation[17], or antifouling properties [18]. The pH responsiveness was introduced either during the membrane formation [19–21] or via a post functionalisation [17,18,22–24]. However, the limitation of these membranes, and materials in general, is that they must be "manually" activated and deactivated by triggering the corresponding stimulus [25]. Materials that cross this boundary gains autonomy, whether it is by allowing self-protection [26], self-reporting [27], self-healing [28], regenerating [29], or controlled degradation ability [30].

A standalone promising feature in this category that has recently been reported is self-oscillation. It involves coupling a sensitive material with a chemical oscillator. A chemical oscillator is a network of chemical reactions in which the concentration of the products changes on a cyclic basis until the source of energy is exhausted. When coupled to a material, continuous periodic variation of macroscopic properties such as its volume or its hydrophobic-hydrophilic balance is observed. Since the first self-oscillating materials developed by Yoshida [31], many works have been carried out with the Belouzov-Zhabotinsky (BZ) oscillator, such as self-walking gel [32], self-oscillating gel for mass transports [33], soft actuators of organized self-oscillating microgels [34] or self-oscillating chemoelectrical interface of solution-gated ion-sensitive field-effect transistor [35]. This concept doesn't allow only to create new materials, but also to discover new possibilities with well-known polymer properties like lower critical solution temperature autonomously modulated by photo-regulation [36]. Despite the accomplishments already reached, the self-oscillating field still has a high potential, with recent progress achieved to precisely control the mechanical oscillation[37,38], or simply by getting even closer to what nature is capable of. Indeed, in all the biological phenomena, the cellular membrane is a wonderful model because of the astonishing possibilities of action, from formation to self-destruction, only triggered by the membrane environment. Being able to reach this complexity level would resolve most of the issues in the membrane field. To achieve this objective, our group recently introduced the concept of self-oscillating filtration membranes [39]. From an alumina membrane functionalized by a pH-sensitive polymer, pH oscillations in the filtration cell made it possible to obtain transmembrane flux oscillations. The principle relies on a change in conformation of a polymer chain as a function of the pH which leads to cycles of opening and closing of the membrane pores.

Here a new strategy is proposed to explore a universal method of introducing self-oscillation functionality to all types of membranes, in particular polymer membranes. The overall strategy is depicted in Figure 1. The

principle is based on the synchronization between a pH oscillator, here Bromate-Sulfite-Ferrocyanide (BSF) and a membrane made pH-sensitive. To obtain this membrane, poly(methacrylic acid) (PMAA) was chosen as a pH-sensitive polymer thanks to its pKa at 4.8 [39]. PMAA is synthesized by Reversible Addition-Fragmentation Chain Transfer (RAFT) polymerization of tert-butyl methacrylate (tBuMA), followed by hydrolysis of the resulting PtBuMA. After aminolysis of the RAFT end group, the PMAA chains are terminated by a thiol function which will be used subsequently for their grafting onto the membrane. To make this grafting possible regardless of the type of membrane, a thin layer of polydopamine is first deposited. A Michael thiol-ene reaction between PMAA and polydopamine then allows membrane functionalisation. In the presence of the pH oscillator, cycles of change in the conformation of the PMAA chains allow for a cyclic change of the pore size and therefore of the transmembrane flux. In this work, the influence of the polydopamine deposition time and the PMAA molecular weight on the oscillation properties is particularly studied.

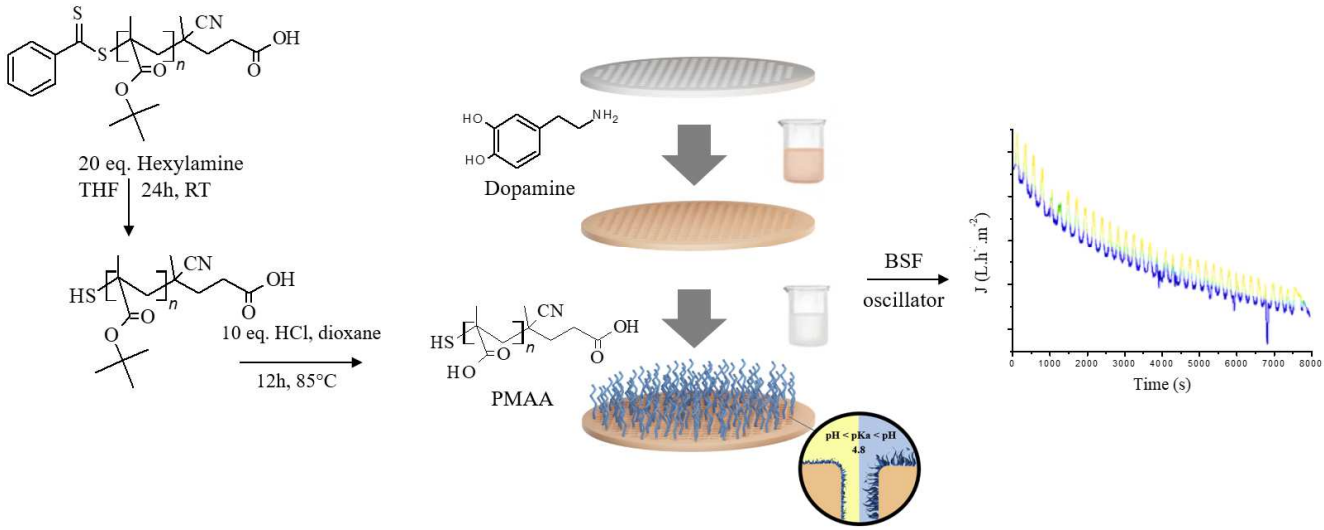

Figure 1 - General strategy carried out to produce self-oscillating polymer membranes

2. Experimental Part

2.1 Materials

Tert-butyl methacrylate 98%, containing 200 ppm monomethyl ether hydroquinone as inhibitor (Sigma) was filtered through an inhibitor removing resin for 15 minutes before use. Azobisisobutyronitrile (Fluka) was used after two recrystallizations in methanol. 4-cyano-4-(phenylcarbonothioylthio)pentanoic acid (Sigma), 1-Hexylamine (Fluka, 99%), chlorohydric acid 37% in weight, (trimethylsilyl)diazomethane solution 2.0 M in diethyl ether (Sigma) dopamine hydrochloride (Sigma), tris glycine buffer solution 10x concentrate (Sigma), potassium bromate (Sigma), bromocresol green, dye content 95% (Sigma), potassium hexacyanoferrate(II) trihydrate (Sigma), sodium sulfite (Sigma), sulfuric acid 99.9% (Sigma), bovine serum albumine (Sigma), dextran from Leuconostoc with Mn= 6000 $g.mol^{-1}$, Mn= 70000 $g.mol^{-1}$, Mn= 100000 $g.mol^{-1}$, Mn= 200000 $g.mol^{-1}$, Mn= 500000 $g.mol^{-1}$, Mn= 2 000000 $g.mol^{-1}$ (Sigma), were used as received. Commercial polyethersulfone membranes with MWCO = 100 kDa, 63.5 mm diameter (Millipore®, PBHK06210) were washed 1 h by immersion in MilliQ water with water being changed three times before use.

2.2. Synthesis and Membrane Functionalisation

2.2.1. RAFT Synthesis of poly(tert butyl methacrylate)

Tert-butyl methacrylate (tBuMA) is placed in a flask with DMF at [tBuMA]= 0.5g.mL^{-1}, and the number of moles of AIBN and CTA corresponding to the target molar mass. As an example, the target ratio for Mn_{PMAA} of 20000 g.mol^{-1} is $\frac{nCTA}{nAIBN}$ = 5 and $\frac{n\ monomer}{nCTA}$ =141. The solution is then degassed with nitrogen in an ice bath for 30 minutes. The reaction was carried out for 24 h at 70 °C. The polymer is then precipitated twice in a cold methanol/water mixture 4:1(v:v) and dried at room temperature under vacuum for 24h.

2.2.2 Aminolysis of poly(tert-butyl methacrylate)

The aminolysis procedure reported by Whittaker and al. [40] was adapted as follows: in a flask, PtBuMa is dissolved at a concentration of 6.5 ml/g in THF and cooled in an ice bath. A large excess of hexylamine ($\frac{n\ hexylamine}{n\ polymer}$ = 20) is cooled in an ice bath. The two solutions are placed in two separate flasks, before being degassed with nitrogen for 30 minutes in an ice bath. The hexylamine solution is added to the polymer solution by syringe under nitrogen flow. The reaction was carried out at room temperature for 20 hours. The polymer is precipitated in a methanol/water mixture 4:1 (v:v) and dried at room temperature under vacuum for 24h.

2.2.3 Deprotection of PtBuMA-SH

The protocol reported by Cazares-Cortes et al. [41] was adapted as follows: aminolyzed PtBuMa is dissolved in dioxane at a concentration [PtBuMA-SH] = 83 mg.mL^{-1}. Under stirring, an excess of HCl ($\frac{n\ HCl}{n\ polymer}$ = 10) is added dropwise, before allowing the reaction to reflux for 16 hours at 85°C. Approximately one third of the solvent was then evaporated on a rotary evaporator before precipitating the polymer in cooled diethyl ether.

2.2.4 Methylation of PMAA to poly(methyl methacrylate) (PMMA)

In order to check the molecular weight distribution of PMAA in organic medium and avoid its aggregation in water during its analysis, PMAA was methylated into poly(methyl methacrylate) (PMMA) before being characterized in Size Exclusion Chromatography in tetrahydrofuran. The protocol reported by Lacik et al. [42] was used and adapted as follows: PMAA is dissolved in a 1:1 (v:v) mixture of THF / water at a concentration of 5mg/mL and placed in a flask. Trimethylsyldiazomethane is then added dropwise with stirring

until the yellow color is constant and no further off-gassing occurs. The flask is left to stir until the solution has completely decolored (7h). The solution was then placed in a beaker in the fume hood and left in the open air until the solvent had evaporated completely.

2.2.5 PDA coating on commercial membranes

The protocol reported by Lee et al. [43] was adapted as follows: in a first step, three 24 mm diameter membranes are cut from the 64 mm commercial membrane, before being washed for 1 hour in Milli-Q water. A pH = 8.5 solution is prepared using a 10: 1 Milli-Q water/tris glycine buffer solution. Dopamine is added to obtain a concentration of 0.1 $mg.mL^{-1}$. Membranes are then immersed 15 minutes directly to the dopamine solution under stirring (70 rpm). Once the reaction is complete, the membrane is washed directly with milli-Q water, then subjected to an ultrasound bath for 15 minutes, and stored in milli-Q water/ethanol 95:5 (v:v).

2.2.6 PMAA-SH grafting on PDA-coated membranes

A 10^{-5} mol solution of PMAA is prepared in milli-Q water at pH = 8.5. The PDA-coated membrane is placed in the solution, and the reaction is carried out at 55°C for 2h. Once the reaction is complete, the membrane is rinsed with milli-Q water, subjected to an ultrasound bath for 15 minutes, and then stored in milli-Q water/ethanol 95 : 5 (v : v).

2.3 Polymer and membrane characterization

2.3.1 Polymer analysis

Proton Nuclear Magnetic Resonance (^{1}H NMR) spectroscopy. The ^{1}H NMR analysis was performed with a Bruker Advance 400 MHz spectrometer. Samples were prepared in deuterated $CDCl_3$ for PtBuMA and MeOD for PMAA.

Size exclusion chromatography (SEC). Molecular weight distributions were assessed by SEC (Viscotek TDA 305, Malvern) using THF as eluent at a flow rate of 1.0 mL/min on a Polymer Laboratories PL-GPC 50 instrument using two PL mixed C 5.0 µm columns at 35 °C and a refractive index detector. Calibration was done using Varian polystyrene narrow standards. Between 1 and 5 mg of polymer was dissolved in 1 ml of a solution of THF with 0.3% toluene (flow marker). The solution was filtered with a 0.22 µm filter before being introduced into the SEC.

Fourier Transform Infrared (FTIR) spectroscopy. FTIR analysis was performed with the FTIR 710 Nicolet instrument (Thermo Electron Corporation). The analyses are performed in ATR mode with 64 scans and a resolution of 82 in transmission mode.

UV-Vis Spectroscopy. Polymer solutions before and after aminolysis were prepared at the same concentration. The analysis was performed in a glass cuvette with the UvLine connect series 940 (SECOMAM) from 200 to 800 nm in absorbance.

2.3.2 Membrane characterization

Water Contact angle (WCA). The WCA analysis was conducted with the ILMS GBX and Digidrop GBX software. The membrane is dried in an oven, before being glued to a support prior the analysis. WCA was measured with a drop volume of approximately 1.7 µL. About 10 measurements are made before being averaged for each trial, and three trials are performed.

Scanning Electron Microscopy (SEM). SEM analyses were conducted using a Hitachi S-4500 (Tokyo, Japan) device operating at spatial resolution of 1.50 nm at 15 kV energy. The samples of 1cm x 0,5 cm were dried and coated with an ultrathin layer of electrically conducting platinum deposited by high-vacuum evaporation. Energy-dispersive X-ray spectroscopy analysis (EDX) was taken with Zeiss EVO HD15 microscope coupled with an Oxford X-MaxNSDD EDX detector. Surface porosity has been obtained from binarized SEM images using Image J® software with $\phi = \frac{\text{Area}_{pores}}{\text{Area}_{total\,surface}} \times 100$.

Gravimetric analysis. Sample gain in weight after functionalization was estimated on samples dried for 1 h in a vacuum oven at 50°C, before being weighed with a Precisa XT 220 A balance.

Porosity measurement. Membranes were previously weighed after drying for 2h in a vacuum oven at 50°C, before being placed under ultrasound for 1 hour in a beaker of 1-butanol until no more bubbles escape from it. The membranes were then weighed directly after removal from the beaker and blotting excess of 1-butanol from the membrane surface. The equation for measuring the porosity (P) is as follows [44]:

$$P(\%) = \frac{(W_2 - W_1)\rho_1}{\rho_1 W_2 + (\rho_2 - \rho_1)W_1}$$

with W_1 = initial mass, W_2 = mass after immersion in 1-butanol, ρ_1 = polyethersulfone density (1.37 g.mol^{-1}) and ρ_2 = 1-butanol density (0.8 g.mol^{-1})

Sieving curves. Dextran of different molecular weights were used to prepare aqueous solutions at a concentration of 1000 ppm. 10 ml was then poured into a dead end stirred filtration cell at 1 bar. The first 2mL of permeated water were discarded, and the next 4mL were taken as permeate solution. The last 4mL remaining in the filtration cell constituted the retentate solution. Membranes were washed 10 minutes in water under ultrasounds between each attempt. The solution signal was then analyzed by a Water 2414 refractive index detector.

Liquid-liquid porometry. It was conducted with PRM-2000-LL-R porometer from G.E.P.S. France. Prior to the measurement, same amount of MilliQ water and 1-butanol was “mixed” and let to separate by decantation in order to saturate the two phases. The aqueous and organic phases were then stored separately.

Before the porometry experiment, the membrane was completely soaked into the aqueous phase before being placed in a porometer cell. Increasing pressure from 0 to 6 bar was applied on the organic phase side of the membrane to progressively replace the aqueous phase.

Zeta potential measurement. The surface charge (zeta potential) of the membrane was estimated using SurPASS electrokinetic analyzer (Anton Paar, GmbH, Graz, Austria) based on the streaming potential method. Washed membrane samples were mounted in an adjustable gap cell and soaked in 1 mM KCl. The cell height was fixed at 100 mm. The electrolyte solution was circulated in the cell between two pieces of membrane. The zeta potential was calculated using the Helmholtz–Smoluchowski equation from the measured streaming current as a function of pH.

X-Ray photoelectron spectrometry (XPS). XPS was carried out with the ESCALAB 250 device from ThermoElectron. The excitation source was the monochromatic source, Al Kα line (1486.6 eV). The surface analyzed has a diameter of 500 µm. Photoelectron spectra were calibrated in binding energy with respect to the energy of the C-C component of carbon C1s at 284.8 eV.

pH analysis. The HI 5221 (Hanna) instrument was calibrated with pH 4, 7 and 9 buffer solutions. Measurements were then recorded every second.

Chemical resistance. Resistance of the membranes to the acidic and alkaline environments was estimated by comparing the initial water flux of the grafted membrane at 1 bar of pressure drop with the flux after an immersion of the membrane during 15 days at pH=3 for acidic condition, and pH=10 for alkaline condition.

Tensile test. Mechanical properties of the membrane were measured with a 5kN ProLine ZwickRoell universal testing machine and screw grips of 10kN. A 1x2cm sample membrane was cut and placed on the screw grip while still wet from the conservation solution. The measurement started with 2cm between the two screw grips.

2.3.3 Water permeation analysis and acquisition of oscillations

The 22 mm diameter membrane was placed into a homemade stainless steel 22 ml dead-end filtration cell. A 1L Amicon tank filled with MilliQ water was connected to the cell with adjustable pressure. Permeated water was measured using a balance connected to the S232 Data Logger software with a 0.599s time step acquisition. A conditioning step was applied to all membranes by applying a pressure drop of 4 bar during 30 minutes before any permeability measurement.

For a water permeation under pH oscillations, aqueous feed solutions separated in two tanks entered premixed at the same flow rate into the dead end filtration cell (Figure SI28) (Tank 1: $[KBrO_3]_0$ = 75 mM and [sodium bromocresol green]$_0$= 2.15 .10^{-3} mM; Tank 2: $[Na_2SO_3]_0$ = 70 mM, $[K_4Fe(CN)_6]_0$ = 15 mM, $[H_2SO_4]_0$ = 7.5 mM). BSF pH oscillator was set up in the filtration cell under pressure and the relative pH evolution was monitored by video acquisition of the solution color change thanks to a pH indicator (bromocresol) (Figure

SI28). The pH oscillator allows cyclic variations of the pH with wide and regular amplitude of oscillations between 3.5 and 6.5 under the membrane filtration conditions (Figure SI24). The targeted k_0 value, which corresponds to the inverse of the residence time in the filtration cell, was 1.10^{-3} s^{-1}.

2.3.4 Modeling of Bromide-Sulfite-Ferrocyanide (pH and ionic strength)

Bromate-sulfite-ferrocyanide (BSF) pH oscillator has been modeled as described in our previous work [39]. The system of Ordinary Differential Equations (ODE) that described chemical reactions was numerically solved using finite element software: COMSOL Multiphysics® 5.4. A variable time step was used to improve the numerical resolution. The evolution of ionic strength (I) during pH oscillations was carried out by taking into account the following ionic species:

Cations: Na^+, H^+, K^+

Anions: OH^-, HSO_4^-, SO_4^{2-}, SO_3^{2-}, HSO_3^-, BrO_3^-, Br^-, $HFe(CN)_6^{3-}$, $Fe(CN)_6^{4-}$

Ionic strength was calculated over time by the following equations:

$$I = \frac{1}{2}\left(\sum_i C_i z_i^2\right)$$

C_i, being the molar concentration of ion i and $z_i$being the charge number of ion i

$$I = \frac{1}{2}([SO_3^{2-}].(-2)^2 + [HSO_3^-].(-1)^2 + [HSO_4^-].(-1)^2 + [SO_4^{2-}].(-2)^2 + [BrO_3^-].(-1)^2 + [Br^-].(-1)^2 + [HFe(CN)_6^{3-}].(-3)^2 + [Fe(CN)_6^{3-}].(-3)^2 + [OH^-].(-3)^2 + [Fe(CN)_6^{4-}].(-3)^2 + [H^+].(1)^2 + [Na^+].(1)^2 + [K^+].(1)^2)$$

Results and Discussion

3.1 Polymer Synthesis

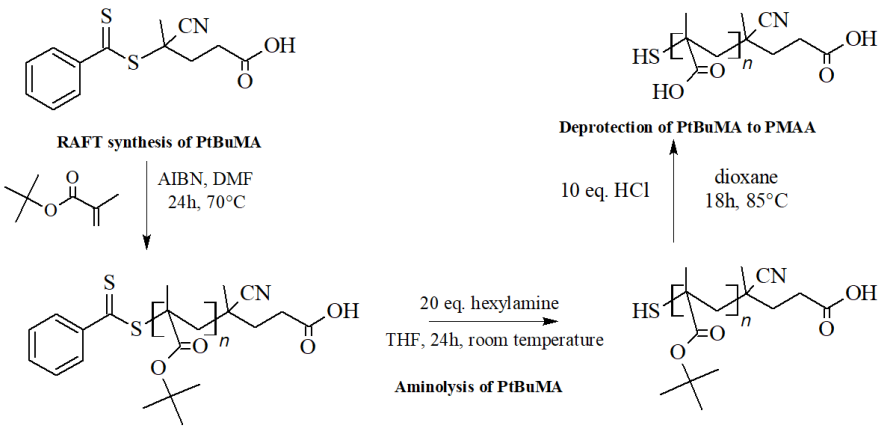

Scheme 1 – Overview of the thiol-functionalized polymethacrylic acid (PMAA) synthesis by RAFT polymerization

3.1.1 RAFT synthesis of PtBuMA

In a first step, a thiolated pH sensitive PMAA was prepared by RAFT polymerization of tBuMA followed by its aminolysis and hydrolysis (Scheme 1). MAA was not polymerized directly as its corresponding PMAA polymer is not soluble in an organic solvent and hard to characterize in water due to its inclination to self-aggregate. The SEC curves of all PtBuMA polymers demonstrate distinct molecular weight distributions and low dispersity as expected from a controlled polymerization (Figure SI-1). PtBuMA was obtained with monomer conversions greater than 70% for all polymers (Table SI-1).

3.1.2 Aminolysis of PtBuMA

As previously explained, the grafting of PMAA onto the polymer membrane was carried out by a Michael thiol-ene reaction on a deposited polydopamine top layer. For that, an aminolysis of the RAFT end group is required to yield a thiol group at the end of the PtBuMa chain (Scheme 1).

The aminolysis was characterized by UV-visible spectroscopy following the absorbance peak at 300 nm, related to the aromatic RAFT end group. A large decrease in the signal attests to the success of the reaction with a yield estimated up to 92% (Figure SI-2a, Table SI-1). The SEC curves before and after aminolysis (Figure SI-2b) demonstrate the integrity of the polymer after the reaction, although some slight chain-chain coupling was observed due to a thiol oxidation into disulphide.

3.1.3 Deprotection of PtBuMA from PMAA

The aminolyzed PtBuMA was then converted into PMAA by hydrolysis of the tert-butyl group. The completion of the reaction is shown by the disappearance of the tert-butyl signal in ^{1}H NMR (Figure SI-6).

The FTIR spectra of the polymers were carried out after each step (Figure SI-3). The PtBuMA and aminolyzed PtBuMA spectra are nearly identical as expected, since the very low concentration of the RAFT end group does not enable any detection. Peak at 2992 cm^{-1} is assigned to the C-H stretching of alkane, and 1735 cm^{-1} to the C=O stretching of ester group. After hydrolysis, FTIR spectrum of the resulting PMAA shows the appearance of a peak at 3300-2500 cm^{-1} assigned to O-H stretching of the carboxylic acid group, as well as a peak at 1715 cm^{-1} corresponding to the C=O stretching of the carboxylic acid group, in agreement with the ^{1}H NMR.

As previously reported [39], PMAA is difficult to characterize in aqueous SEC due to the presence of aggregates. To check the distribution of molecular weights after hydrolysis of the tert-butyl group, PMAA was methylated in poly(methyl methacrylate) (PMMA) and analyzed in THF SEC (Figure SI-4). A shift of the entire distribution toward lower molecular weights is observed, as expected, with a maintained low dispersity of 1.06. Note that the secondary pic corresponds to a double molecular weight, which is due to thiol-thiol coupling, as explained before.

3.2 Membrane functionalisation

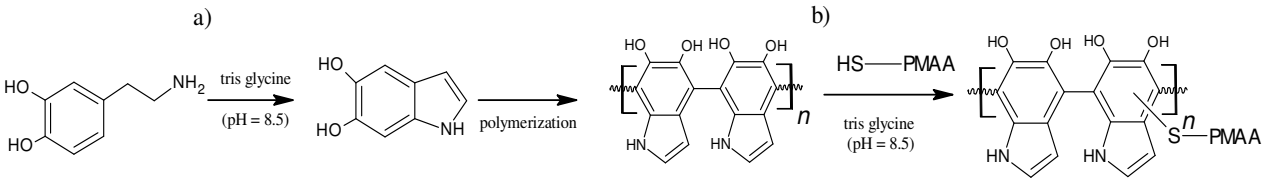

Figure 2 – a) Synthesis and coating of polydopamine onto polyethersulfone membrane followed by b) grafting of pH-sensitive PMAA chains through Michael thiol-ene reaction.

The functionalisation of a commercial polyethersulfone membrane (PES) by the pH sensitive PMAA was mediated through the deposition of a thin polydopamine (PDA) layer, as described in Figure 2. This technique, already reported in the literature [45], is very versatile and can be applied to all types of membranes without physicochemical constraints due to the ability of the PDA to stick anywhere. Polymer grafting was then performed simply by immersion of the PDA-coated membrane in a PMAA solution. This functionalisation process occurs in water under mild conditions, making any potential scale-up environmentally friendly.

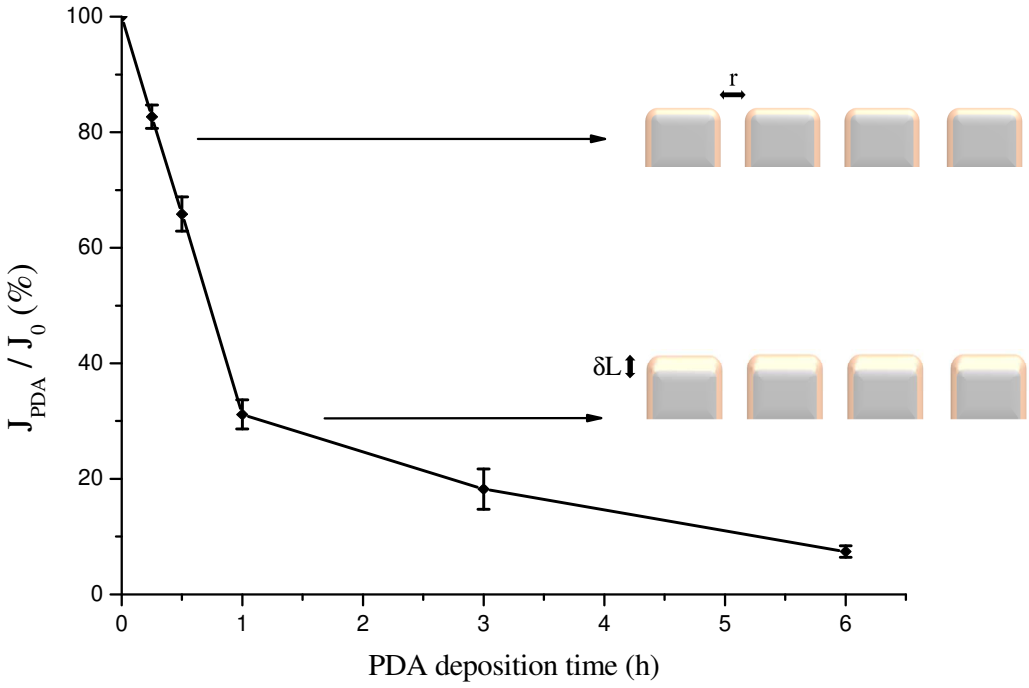

312 Figure 3 – Evolution of the flux of the PES membrane after PDA deposition (J_{PDA}) compared to the flux of the
313 virgin membrane (J_0).

314

315 The permeance of the PDA coated membranes in Figure 3 shows a decrease correlated with the
316 deposition time. In a first part, delimited by a PDA deposition time of less than 1 hour, a significant slope is
317 observed while a clear break beyond this time marks a slower evolution. This distinction can illustrate two
318 different flux reduction mechanisms. As the Poiseuille equation (1) shows, the flux can evolve by a change in the
319 radius of the pores (to the power of 4), their number, and their length. Given the rapid evolution for short
320 deposition times, we can hypothesize that a decrease in the pore diameter is the main factor involved in this first
321 part. Then, the PDA coating increasing with time, the length of the pores, and the number of open pores certainly
322 govern the evolution of the flux in the second part.

323 $$J = \frac{N.dP.r^4}{8.\eta.L} \qquad (1)$$

324 with J = transmembrane flux; N = pores number; dP = pressure gradient across the membrane; r = average pore
325 radius; L = membrane thickness; η = fluid viscosity.

326 A 15 min deposition time was selected for the rest of the work, which is a good compromise between enough
327 PDA functionalisation for the subsequent PMAA grafting and moderate flux decrease.

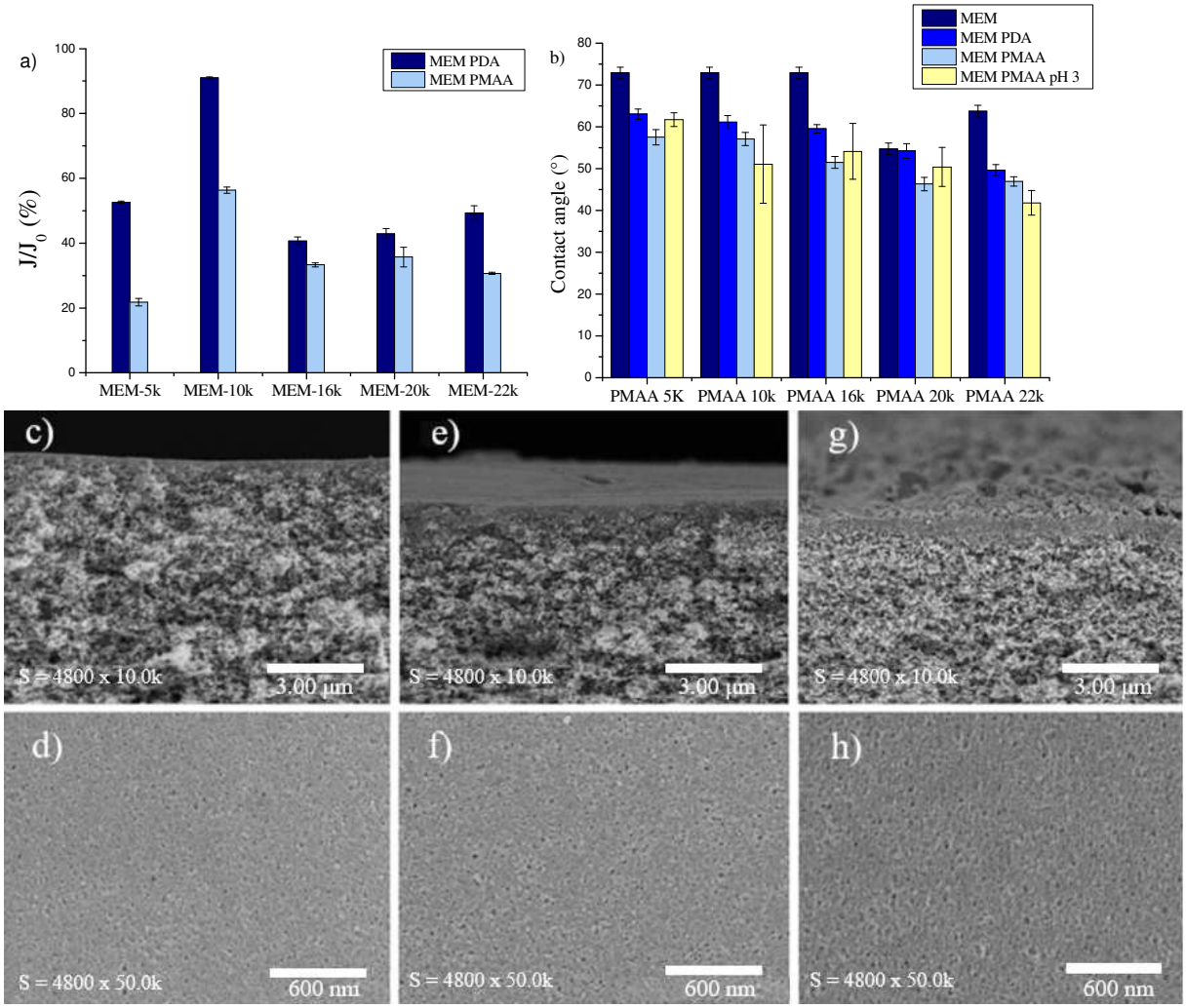

Figure 4 –a) Evolution of the flux (J) after PDA deposition and after PMAA grafting as normalized by the flux of the virgin membrane (J_0), as a function of PMAA molecular weight, b) Water contact angle on virgin PES membrane (MEM), PDA modified membrane (MEM PDA) and PMAA grafted membrane (MEM PMAA), c-h) SEM images of cross sections (c, e, g) and top surfaces (d, f, h) of virgin PES membrane (c, d), 15 min PDA coated PES membrane (e, f), and $PMAA_{22k}$ grafted membrane (g, h).

The functionalisation was indirectly characterized by the flux measurement (Figure 4a). A flux decrease is observed after each functionalisation step from virgin PES membrane to PDA-modified membrane to PMAA-grafted membrane. However, the decrease does not appear to be correlated with the molecular weight of the grafted PMAA and ranges from 10 to 60% for the same PDA deposition time (15 min).

An increase of the surface hydrophilicity was also observed after each step, illustrated by the decrease of the water contact angle (Figure 4b). If the trend is clear and constant, the water contact angle seems to be sample dependent, with a dependence more relying on the varying surface roughness rather than the results of the PMAA molecular weight for instance. Switching the water pH of the droplets from 7 to 3 did not provide a clear tendency. It is assumed that it is the result of two antagonist effect: an acidic pH below the PMAA pKa will

result in the pore opening due to the polymer contraction. However, PMAA also became less hydrophilic at this pH, as did the membrane surface.

Each step of membrane modification has been characterized by SEM (Figure 4c-h). Although the top surface images do not show any real difference after functionalization steps, a thin layer of PDA and PMAA is well observed in the cross-section images. The EDX mapping (Figure SI-8) shows that PMAA is uniformly grafted with visible enrichment of carbon on the surface. The membrane bulk porosity was estimated from 1-butanol gravimetric analysis and a stable value around 77% is found for all membranes (porosity $_{MEM}$ = 77.5%; porosity $_{MEM\ PDA\ 15\ min}$ = 77.7%; porosity $_{MEM\ PMAA\_10k}$ = 77.2%). Since only a surface modification is performed on an asymmetric PES membrane, the overall porosity is in return not affected. On the contrary, the time of PDA deposition is found to change surface porosity, as measured by SEM image treatment (porosity $_{MEM}$ = 7.8%; porosity $_{MEM\ PDA\ 15\ min}$ = 3.4%; porosity $_{MEM\ PDA}$ 1 h = 3.5%; porosity $_{MEM\ PDA}$ 18 h = 1.5%). Similar trend is observed with PMAA grafting, which reduces surface porosity (porosity $_{MEM\ PMAA\_22k\ (with\ PDA=15\ min)}$ = 2.3%), in agreement with a polymer coating/grafting.

Gravimetric analysis was carried out to estimate the weight of polymer deposited at the membrane surface after PDA coating and PMAA grafting (Table SI-3). As expected, a correlation between the PDA deposition time and the PDA quantity deposited is observed. Because PMAA is grafted onto the PDA layer, a direct link is observed between the quantity of PDA deposited and the yield of PMAA grafting. Interestingly, for the same PMAA grafting time, the grafted PMAA was 2.4 times higher when the deposited PDA was higher. Here it is suspected that 18h PDA coating has increased surface roughness and thus the specific PDA surface available for PMAA grafting. Young moduli (tensile test) were measured to see if the PMAA grafting would have an impact, but it appears that the deposition is too thin to make any significant difference (Table SI-4).

The surface composition was characterized by XPS analysis (Figure SI-9-19). However, unless a sufficient PDA layer is deposited (18h), the elemental compositions (C, N, O and S) of the PDA coated membranes remain similar to the PES commercial membrane. This is a further proof that the PDA deposition time chosen (15 minutes) allows a very thin layer to be deposited, sufficient to be able to functionalize without drastically changing the chemical nature of the interface. The XPS data (Table SI-5) shows that the carbon and nitrogen concentrations in PMAA grafted membranes are similar than in the commercial membrane, but the oxygen concentration rises with the polymer grafting, which is in line with the theory. It also appears that the sulfur concentration decreases for all the grafted samples, proving that deposition on the PES membrane is taking place.

A measurement of the streaming potential was performed (Figure SI-7). A significantly different evolution of the calculated negative zeta potential is observed, attesting to the difference in surface chemistry. However, a similar isoelectric point (IEP) at pH 3-3.5 for the three samples, in agreement with reported PES IEP[46], suggests that only a partial coverage of the membrane surface occurs.

3.3 pH-induced self-oscillating flux

In order to yield a self-oscillating behavior, a pH-sensitive polymer membrane is mounted into a dead-end filtration cell and synchronized with a pH oscillator (Figure SI-26). PMAA is a weak polyelectrolyte with a quick conformation change as a function of pH. A globular conformation is observed for low degrees of ionization, and the chains are collapsed due to the "hydrophobic" interactions with the methyl groups. The membrane pores are then in an "open" state. The polymer chains expand abruptly above a pH threshold (pKa = 4.8) to release the electrostatic energy associated with deprotonation. The membrane pores are "closed" at this point. The BSF pH oscillator can generate pH cycles ranging from 3.5 to 6.5 (Figure SI-22). The BSF oscillator and the pH-sensitive membrane must be synchronized in order for the membrane pores to vary cyclically and to thus observe a periodic variation of the transmembrane flux. The first step is to check the "unresponsiveness" of the virgin PES membrane to pH in terms of water permeability. Thus, the virgin PES membrane was subjected to sequential pH variations (3 and 7) (Figure SI-20). Ignoring the effect of the depressurization of the filtration cell during the change of solutions, no significant change in flux was observed in relation to the pH. One can note a natural tendency of transmembrane flux decrease over time despite the conditioning performed (see experimental part for more details).

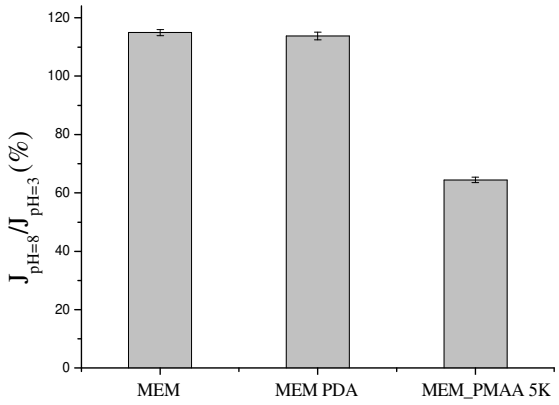

Figure 5 – Water flux ratio at pH 8 and 3 of the commercial PES membrane (MEM), the membrane coated with PDA for 15 min (MEM PDA), and the membrane grafted with $PMAA_{5k}$ (MEM_ $PMAA_{5k}$) at ΔP= 1 bar.

The pure water flux of the virgin PES membrane, the PDA coated membrane, and the PMAA grafted membrane were then measured at pH values above and below the PMAA pKa to assess its effect (Figure 5). Whereas a slight increase in flux at basic pH is observed for commercial and PDA covered membranes, a clear flux decreases of 40% at pH=8 is measured when PMAA is grafted onto the membrane. Indeed, above PMAA pKa value, the polymer is in an expanded conformation which obstructs the pores and reduces their size. Since the dependence is inversed compared to the PDA coated membrane, it can be deducted that PMAA membrane is pH-sensitive and that a modulation of the pH results in a proportionate change in the water permeability. It should be noted that the tolerance of the membrane towards acidic and alkaline operating conditions was checked to avoid any misinterpretation. The water flux at ΔP = 1 bar of the virgin PES membrane and the PMAA grafted membrane was measured at pH 3 and 10 for 15 days without showing any significant change ($J_{PES\ MEM,\ pH3}$=278±51 $L.h^{-1}.m^{-2}$; $J_{PES\ MEM,\ pH10}$=181±24 $L.h^{-1}.m^{-2}$; $J_{PMAA\ MEM,\ pH3}$=125±3 $L.h^{-1}.m^{-2}$; $J_{PMAA\ MEM,\ pH10}$=129±5 $L.h^{-1}.m^{-2}$).

As explained before, autonomous cyclic pH change will be carried out thanks to the BSF chemical oscillator setup in the filtration cell. BSF is an oscillating network of chemical reactions, which can be summarized by a set of 7 reactions [39] (Table SI-6). The cyclic predominance of certain reactions in the BSF oscillator leads to a modulation of the pH within a domain of residence time in the filtration cell. The residence time domain to observe the pH oscillations was previously estimated from the construction of a bifurcation diagram (Figure SI-21) [39] and a k_0 value of 10^{-3} s^{-1} was targeted in this work, k_0 being the inverse of the residence time in the filtration cell. The pH oscillations produced from a BSF oscillator for a k_0 of 10^{-3} s^{-1} have an average period of about 390 s after stabilization with a pH varying cyclically and continuously between 3 and 6.5 (Figure SI-22). PMAA pKa being around 4.8, then the pH oscillations will enable change of conformation of PMAA chains grafted on the membranes. Because of the inability to directly follow the pH change in a pressurized filtration cell, a colored indicator was used to visually track the pH oscillation. The BSF reaction alone was filmed and monitored by a pH-meter to see if the colored indicator is a reliable tracking system

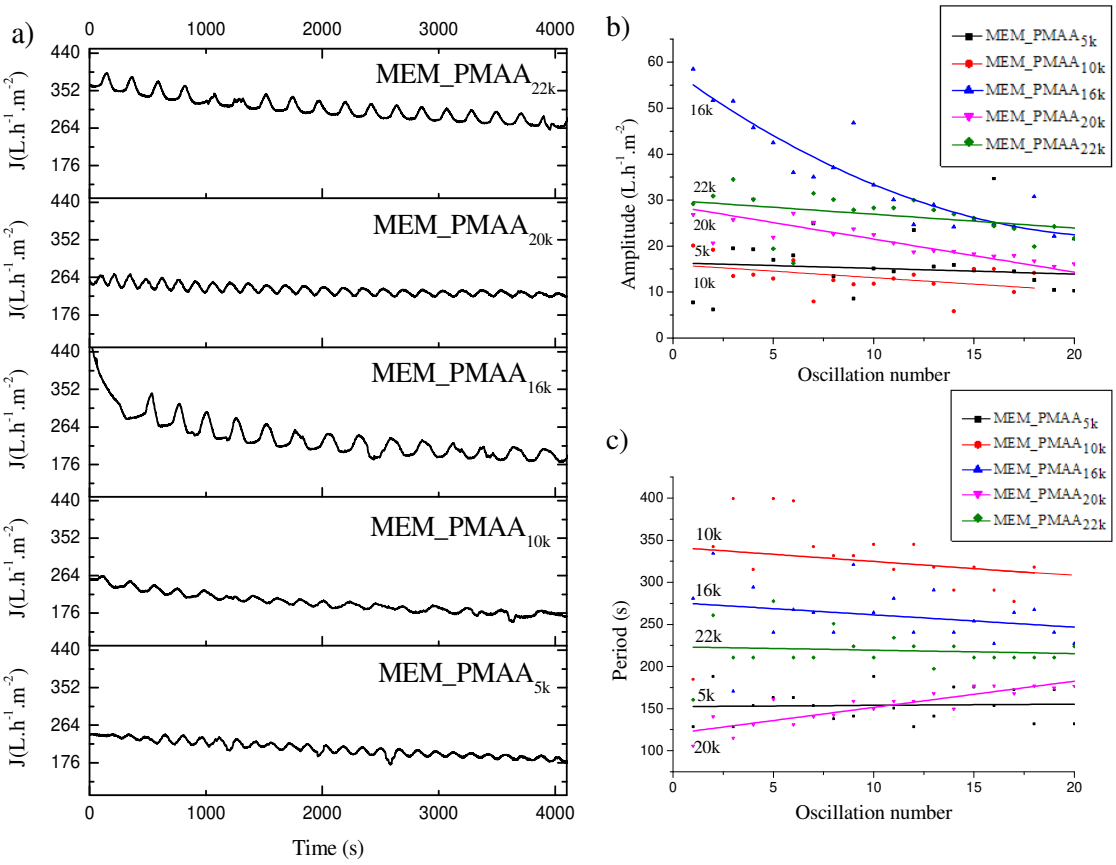

(Figure SI-23). It appears that the visual color change and the pH change match perfectly.

Figure 6 – a) Self-oscillating flux of functionalized membranes synchronized with a BSF oscillator with the following conditions: $[KBrO_3]_0$ =75 mM, $[Na_2SO_3]_0$ =70 mM, $[K_4Fe(CN)_6]_0$ = 15 mM, $[H_2SO_4]$ = 7.5 mM for T

= 30 °C and $k_0 = 10^{-3}$ s^{-1}; b) Evolution of oscillation amplitude for each PMAA molecular weight; c) Evolution of oscillation period for each PMAA molecular weight. b-c) Fitting curves are shown only as a guide for the eye

When the BSF pH oscillator is set up in the filtration cell with PMAA-functionalised PES membranes, flux oscillations are observed as shown in Figure 6a. It appears that the molecular weight of PMAA greatly affects the flux oscillations, as much in amplitude than in period. Also, the BSF oscillator seems to be able to have a great stability under filtration conditions as self-oscillating flux could still be recorded after 35 cycles of pH (Figure SI-27). Figure 6b shows that there is a more or less pronounced decrease of the oscillation amplitude in time, with a variable intensity depending on the PMAA molecular weights. The PMAA chains remain hydrophilic all the time including below the pKa of the PMAA. However, as reported in literature, the grafted polymer onto the membrane surface may not be fully accessible to the bulk solution and some charges can remain avoiding a complete polymer collapsing over the cycles [47]. It can be noted that the greatest decrease in amplitude was observed with MEM_PMAA16k. The oscillation periods represented in Figure 6c remain relatively stable over time, except for MEM_PMAA20k, for which a slight increase is observed over time. As the oscillation period depends on the oscillator mechanism, it is complex to analyse the evolutions. However, it appears that all the periods are shorter than for the BSF oscillator alone, which shows that the membrane participates in the oscillating system. The molecular weight of the grafted PMAA appears to modulate both the period and the amplitude, as summarized in Figure 7.

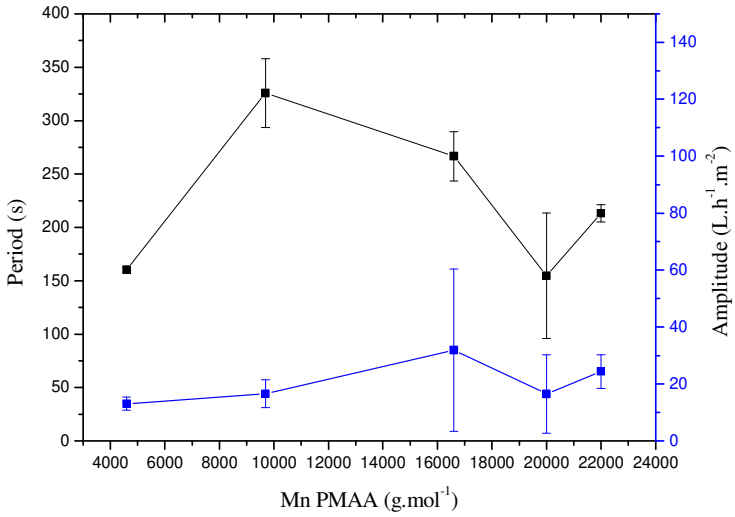

Figure 7 - Average amplitude and period of water flux oscillations for each PMAA molecular weight

When the two parameters are compared in Figure 7, it appears that both values increase with the molecular weight of PMAA, then decrease for $PMAA_{20k}$, before increasing again at $PMAA_{22k}$. A hypothesis is that a steric exclusion occurs between Mn= 16 000 g.mol^{-1} and 20 000 g.mol^{-1}. A large amplitude can be observed when the PMAA is located inside the pores. When the PMAA chain length is increased, the flux change, corresponding to the compact and extended conformations of PMAA in the pores, is larger. However, above a threshold value of PMAA molecular weight, some steric hindrance can occur, preventing grafting inside the pores and thus leading to a decrease in the flux oscillation amplitude. A second increase above 20 000 g.mol^{-1} is also observed which can be explain by an obstruction of the pores from the membrane surface. If the

hypothesis is correct, the pore size distribution for MEM_PMAA$_{10k}$ and MEM_PMAA$_{20k}$ would be significantly different. Indeed, MEM_PMAA$_{10k}$ would have a reduced pore size due to the presence of the polymer chains in the pores, whereas grafting of MEM_PMAA$_{20k}$ would have a lower pore size impact, being mostly located at the membrane surface. The sieving curves, carried out with dextran of different molecular weights, are presented in Figure 8.

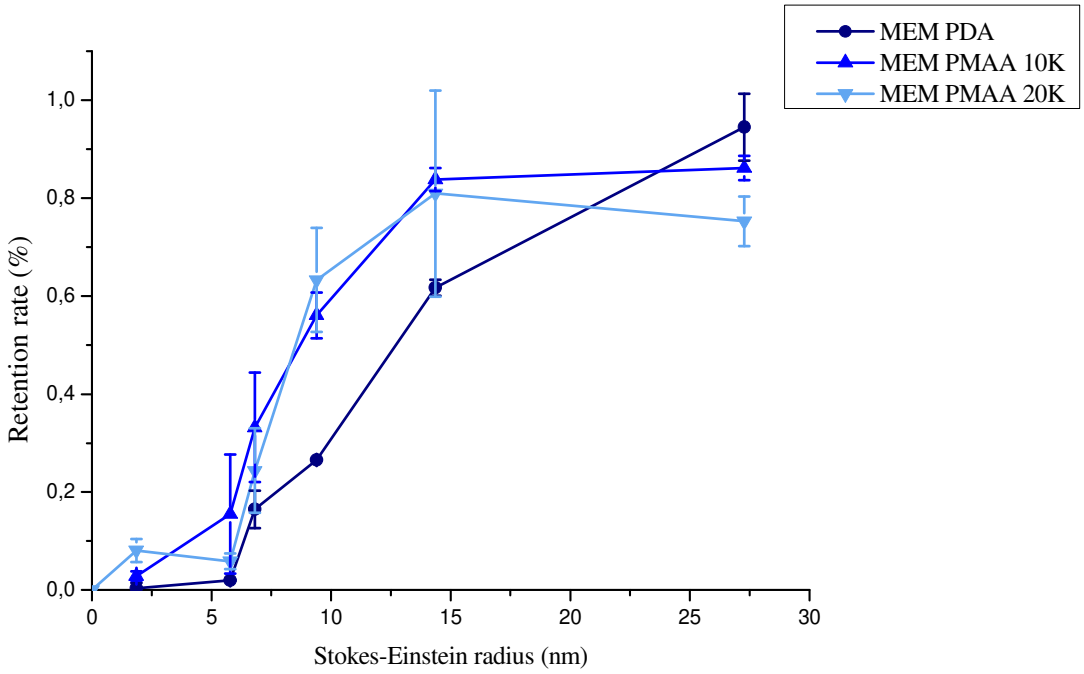

Figure 8 – Sieving curve for ●) PDA coated membrane ▲) grafted membrane with PMAA =10 000 g.mol^{-1} and ▼) grafted membrane with PMAA =20 000 g.mol^{-1}

The sieving curves were measured for two grafted PMAA molecular weights, PMAA$_{10k}$ and PMAA$_{20k}$. It should be first mentioned that a weak reproducibility was observed when repeating the sieving curve measurements on different samples of the same membrane as illustrated by the large error bars obtained for the virgin PES membrane (Figure SI-28) [48]. To try to overcome its impact, the sieving curves were made on the same membrane for all the functionalisation steps (Figures 8). It appears that the PDA deposition has not clearly shifted the sieving curve towards lower pore values as expected, which could be explained by a change in the surface properties (hydrophilicity, roughness) counterbalancing the pore size decrease. Grafting of PMAA has shifted the sieving curve to lower pore size, in agreement with the flux decrease observed previously. However, considering the error bars, the sieving curves as measured with the two PMAA molecular weights did not highlight a significant difference.

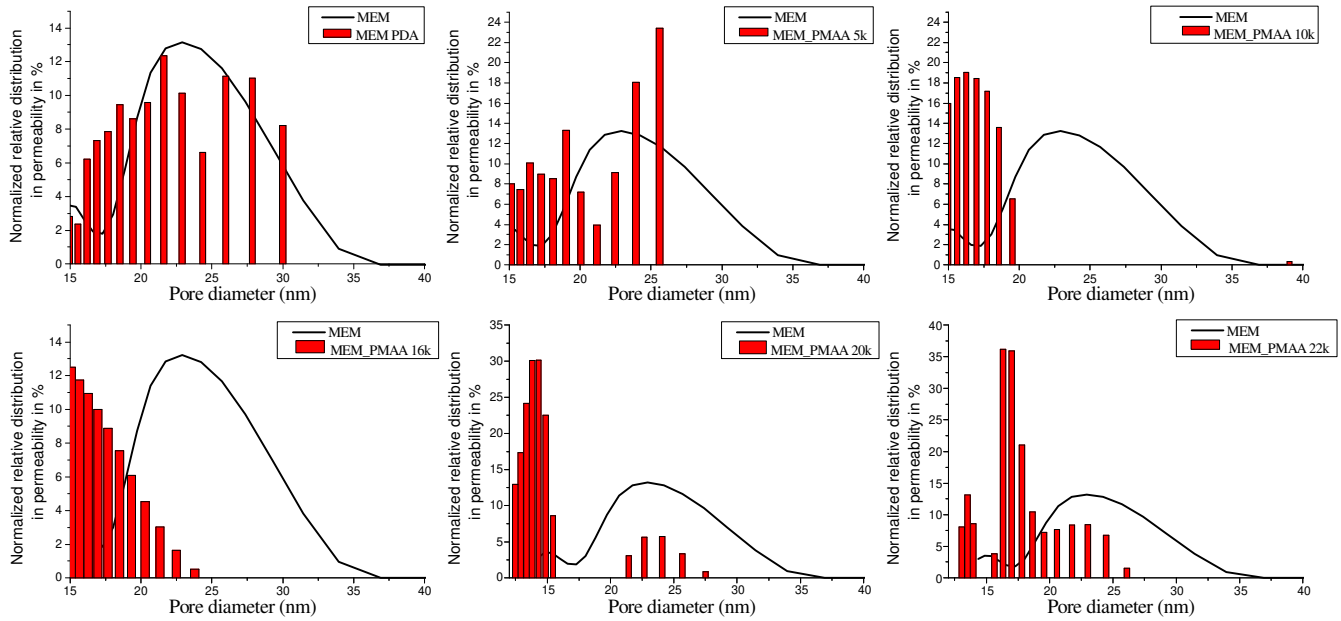

Figure 9 – Liquid-liquid porometry results for PES commercial membrane, PDA-coated membrane (15 min) and membranes grafted with PMAA of different molecular weights.

Liquid-liquid porometry (Figure 9) shows that the commercial membrane has an average pore size of 22 nm and a relatively large dispersity. The PDA deposition doesn't seem to affect significantly the pore size distribution. However, when PMAA is grafted, the pore size distribution is shifted towards lower values in all cases, showing that PMAA grafting is decreasing the pore size with a higher shift towards lower pore size with increasing PMAA molecular weight, in agreement with the evolution of the water flux as previously discussed. However, for the membranes grafted with PMAA $\geq$ 20 000 g.mol^{-1}, a double distribution is observed with smaller pores as in the case observed with PMAA lower than 20 kg.mol^{-1}, but also with a remaining distribution of pore size from the initial PDA membrane. A hypothesis is that a partial steric exclusion of PMAA from the membrane pores appended leading to leave unfunctionalized a part of the initial pore size distribution. This is in agreement with the break in water flux amplitude trend observed in Figure 7 at this PMAA molecular weight. We didn't succeed in showing a clear shift of the pore size distribution from the sieving curves or from the porometry measurement when comparing the results at pH below and above the PMAA pKa (data not shown). To understand that observation, the expected pore size variation resulting from a pH below and above the PMAA pKa was estimated from the measured water flux variations according to the Poiseuille law (equation 1) (Table SI-7).

A pore size change of maximum 2.5 to 6.5% (0.4 to 1.5 nm) is expected which explains the difficulty to directly observe it following the pore size. It is however clearly visible in the flux measurement thanks to dependence of the flux to the fourth power of the pore radius. We can therefore conclude that water flux self-oscillations have been yielded without significantly alter the solute retention of membrane.

The BSF oscillator involves many ionic species whose concentration can vary with time depending on the oscillatory regime. Given our use of a weak polyelectrolyte (PMAA), the impact of ionic strength on water permeation results was checked. For this, the ionic strength of the oscillator (400 mmol.L^{-1}) was reproduced by adding NaCl (0.4 mol.L^{-1}) to water. As shown in Figure SI-25, the transition from pure water to salted water was

not accompanied by a change in flux. In addition, a theoretical modeling of pH and ionic strength oscillations was performed (Figure SI-24) and only a weak ionic strength oscillation is observed between 414 and 420 $mmol.L^{-1}$. Thus, we can conclude that the ionic strength imposed by the pH oscillator does not impact the water permeation results. The flux oscillations are therefore only the results of the expansion-contraction cycles of the PMAA inside the membranes pores.

3. Conclusions

Self-oscillating polymer membranes showing continuous periodic flux evolution have been successfully prepared. The flux oscillations were obtained by coupling a pH-sensitive polymer membrane to a pH oscillator (BSF). For this, PMAA was synthesized with different molecular weights and grafted onto a commercial PES membrane via an intermediate layer of PDA. Each stage of polymer manufacturing and membrane functionalisation has been precisely characterized. Secondly, the pH oscillator was stabilized in a filtration cell and brought into contact with the pH-sensitive membrane. The PMAA grafted onto the membrane responds almost instantaneously to changes in pH and oscillates between two chain conformations (extended and collapsed). Therefore, an autonomous and cyclic membrane pore size change was observed leading to the self-oscillation of the membrane water flux. Interestingly, although water flux is periodically modulated, the corresponding pore size change due to the pH modulation is estimated to be less than 6%, which has immeasurable impact on the solute retention of membrane. In addition, the amplitude of the flux cycles can be modulated by the molecular weight of the PMAA grafted onto the membrane until a threshold value of 20 000 $g.mol^{-1}$, above which a polymer exclusion from the pores was observed. In perspective to this work, the effect of flux oscillations on the challenging fouling phenomenon will be explored since a perpetual change of the membrane surface properties combined with an adhesion of retained species hampered by flux oscillations could offer a more sustainable alternative to the usual mechanical and chemical membrane cleanings. Bringing self-oscillating behaviour to a polymer filtration membrane represents a further step towards the design of autonomous membranes.

Credit authorship contribution statement

Johanne Pirkin-Benameur: Conceptualization, Methodology, Data curation, Writing – original draft, Writing – review & editing. **Denis Bouyer**: Conceptualization, Methodology, Data curation. **Damien Quemener**: Conceptualization, supervision, acquisition of funds, data curation, writing - review & editing.

Declaration of Competing Interest

The authors declare no conflict of interest.

Acknowledgements

The authors thank the Institut Universitaire de France (IUF) and the Agence Nationale de la Recherche (ANR) through the OsciMEM project (ANR-20-CE06-0013-01) for financial support. Valérie Flaud, Didier Cot, and Bertrand Rebiere are acknowledged for XPS, SEM, and EDX analysis.

References

[1] L. Persson, B.M.C. Almroth, C.D. Collins, S. Cornell, C.A. de Wit, M.L. Diamond, P. Fantke, M. Hassellöv, M. MacLeod, M.W. Ryberg, P.S. Jørgensen, P. Villarrubia-Gómez, Z. Wang, M.Z. Hauschild, Outside the Safe Operating Space of the Planetary Boundary for Novel Entities, Environmental Science & Technology. (2022) acs.est.1c04158. https://doi.org/10.1021/ACS.EST.1C04158.

[2] M. Wei, Y. Gao, X. Li, M.J. Serpe, Stimuli-responsive polymers and their applications, Polymer Chemistry. 8 (2016) 127–143. https://doi.org/10.1039/C6PY01585A.

[3] D. Roy, W.L. A. Brooks, B. S. Sumerlin, W.L.A. Brooks, B.S. Sumerlin, New directions in thermoresponsive polymers, Chemical Society Reviews. 42 (2013) 7214–7243. https://doi.org/10.1039/C3CS35499G.

[4] S. Dai, P. Ravi, K. Chiu Tam, K.C. Tam, {pH}-Responsive polymers : synthesis, properties and applications, Soft Matter. 4 (2008) 435–449. https://doi.org/10.1039/B714741D.

[5] D.A. Davis, A. Hamilton, J. Yang, L.D. Cremar, D. Van Gough, S.L. Potisek, M.T. Ong, P. V. Braun, T.J. Martínez, S.R. White, J.S. Moore, N.R. Sottos, Force-induced activation of covalent bonds in mechanoresponsive polymeric materials, Nature 2009 459:7243. 459 (2009) 68–72. https://doi.org/10.1038/nature07970.

[6] Y.L. Colson, M.W. Grinstaff, Y.L. Colson, M.W. Grinstaff, Biologically Responsive Polymeric Nanoparticles for Drug Delivery, Advanced Materials. 24 (2012) 3878–3886. https://doi.org/10.1002/ADMA.201200420.

[7] A. Fernández-Nieves, Engineering colloids with optical and geometrical anisotropies: de-coupling size monodispersity and particle properties, Soft Matter. 2 (2006) 105–108. https://doi.org/10.1039/B512441G.

[8] N.S. Terefe, O. Glagovskaia, K. De Silva, R. Stockmann, Application of stimuli responsive polymers for sustainable ion exchange chromatography, Food and Bioproducts Processing. 92 (2014) 208–225. https://doi.org/10.1016/J.FBP.2014.02.003.

[9] G.W. De Groot, M.G. Santonicola, K. Sugihara, T. Zambelli, E. Reimhult, J. Vörös, G.J. Vancso, Switching transport through nanopores with pH-responsive polymer brushes for controlled ion permeability, ACS Applied Materials and Interfaces. 5 (2013) 1400–1407. https://doi.org/10.1021/AM302820Y/SUPPL_FILE/AM302820Y_SI_001.PDF.

[10] X. Gao, W. Yang, P. Pang, S. Liao, Q. Cai, K. Zeng, C.A. Grimes, A wireless magnetoelastic biosensor for rapid detection of glucose concentrations in urine samples, Sensors and Actuators B: Chemical. 128 (2007) 161–167. https://doi.org/10.1016/J.SNB.2007.05.045.

[11] D. Schmaljohann, Thermo- and pH-responsive polymers in drug delivery, Adv Drug Deliv Rev. 58 (2006) 1655–1670. https://doi.org/10.1016/J.ADDR.2006.09.020.

[12] X. Yang, L. Chen, B. Huang, F. Bai, X. Yang, Synthesis of pH-sensitive hollow polymer microspheres and their application as drug carriers, Polymer (Guildf). 50 (2009) 3556–3563. https://doi.org/10.1016/J.POLYMER.2009.06.027.

[13] P. Zarrintaj, M. Jouyandeh, M.R. Ganjali, B.S. Hadavand, M. Mozafari, S.S. Sheiko, M. Vatankhah-Varnoosfaderani, T.J. Gutiérrez, M.R. Saeb, Thermo-sensitive polymers in medicine: A review, European Polymer Journal. 117 (2019) 402–423. https://doi.org/10.1016/J.EURPOLYMJ.2019.05.024.

[14] J.B. Qu, L.Y. Chu, M. Yang, R. Xie, L. Hu, W.M. Chen, A pH-Responsive Gating Membrane System with Pumping Effects for Improved Controlled Release, Advanced Functional Materials. 16 (2006) 1865–1872. https://doi.org/10.1002/ADFM.200500897.

[15] G. Yi, X. Fan, X. Quan, H. Zhang, S. Chen, H. Yu, A pH-responsive PAA-grafted-CNT intercalated RGO membrane with steady separation efficiency for charged contaminants over a wide pH range, Separation and Purification Technology. 215 (2019) 422–429. https://doi.org/10.1016/J.SEPPUR.2019.01.028.

[16] Z. Chen, M.H.-Y. Chan, V.W.-W. Yam, Stimuli-Responsive Two-Dimensional Supramolecular Polymers Based on Trinuclear Platinum(II) Scaffolds: Reversible Modulation of Photoluminescence, Cavity Size, and Water Permeability., J Am Chem Soc. (2020). https://doi.org/10.1021/jacs.0c07969.

[17] Q. Ye, R. Wang, C. Chen, B. Chen, X. Zhu, High-Flux pH-Responsive Ultrafiltration Membrane for Efficient Nanoparticle Fractionation., ACS Applied Materials & Interfaces. (2021). https://doi.org/10.1021/acsami.1c16673.

[18] Z. Ma, G. Shu, X. Lu, Preparation of an antifouling and easy cleaning membrane based on amphiphobic fluorine island structure and chemical cleaning responsiveness, Journal of Membrane Science. (2020). https://doi.org/10.1016/j.memsci.2020.118403.

[19] J. Qiao, L. Liu, J. Shen, L. Qi, Enzyme immobilization on a pH-responsive porous polymer membrane for enzymatic kinetics study, Chinese Chemical Letters. 32 (2021) 3195–3198. https://doi.org/10.1016/J.CCLET.2021.03.021.

[20] K. Aissou, H. Bouzit, F. Krusch, J.P. Méricq, D. Cot, N. Masquelez, S. Roualdes, D. Quémener, Asymmetric Solvent-Annealed Triblock Terpolymer Thick Films Topped by a Hexagonal Perforated Lamellar Nanostructure, Macromol Rapid Commun. 43 (2022). https://doi.org/10.1002/MARC.202100585.

[21] T. Luo, S. Lin, R. Xie, X.J. Ju, Z. Liu, W. Wang, C.L. Mou, C. Zhao, Q. Chen, L.Y. Chu, pH-responsive poly(ether sulfone) composite membranes blended with amphiphilic polystyrene-block-poly(acrylic acid) copolymers, Journal of Membrane Science. 450 (2014) 162–173. https://doi.org/10.1016/J.MEMSCI.2013.09.002.

[22] H. Salehi, A. Shakeri, H. Mahdavi, R.G.H. Lammertink, Improved performance of thin-film composite forward osmosis membrane with click modified polysulfone substrate, Desalination. (2020). https://doi.org/10.1016/j.desal.2020.114731.

[23] M.G. Kochameshki, M. Mahmoudian, A. Marjani, K. Farhadi, M. Enayati, H.S. Mollayousefi, Graphene oxide grafted poly(acrylic acid) synthesized via surface initiated RAFT as a pH-responsive additive for mixed matrix membrane, Journal of Applied Polymer Science. (2019). https://doi.org/10.1002/app.47213.

[24] X. Deng, J.L. Livingston, N.J. Spear, G.K. Jennings, PH-Responsive Copolymer Films Prepared by Surface-Initiated Polymerization and Simple Modification., Langmuir. (2020). https://doi.org/10.1021/acs.langmuir.9b03026.

[25] A. Walther, A. Walther, Viewpoint: From Responsive to Adaptive and Interactive Materials and Materials Systems: A Roadmap, Advanced Materials. 32 (2020) 1905111. https://doi.org/10.1002/adma.201905111.

[26] T.S. Wong, S.H. Kang, S.K.Y. Tang, E.J. Smythe, B.D. Hatton, A. Grinthal, J. Aizenberg, Bioinspired self-repairing slippery surfaces with pressure-stable omniphobicity, Nature 2011 477:7365. 477 (2011) 443–447. https://doi.org/10.1038/nature10447.

[27] G.R. Gossweiler, G.B. Hewage, G. Soriano, Q. Wang, G.W. Welshofer, X. Zhao, S.L. Craig, Mechanochemical activation of covalent bonds in polymers with full and repeatable macroscopic shape recovery, ACS Macro Letters. 3 (2014) 216–219. https://doi.org/10.1021/MZ500031Q/SUPPL_FILE/MZ500031Q_SI_002.PDF.

[28] X. Chen, M.A. Dam, K. Ono, A. Mal, H. Shen, S.R. Nutt, K. Sheran, F. Wudl, A thermally re-mendable cross-linked polymeric material, Science (1979). 295 (2002) 1698–1702. https://doi.org/10.1126/SCIENCE.1065879/SUPPL_FILE/1065879S3_THUMB.GIF.

[29] S.R. White, J.S. Moore, N.R. Sottos, B.P. Krull, W.A. Santa Cruz, R.C.R. Gergely, Restoration of large damage volumes in polymers, Science (1979). 344 (2014) 620–623. https://doi.org/10.1126/SCIENCE.1251135/SUPPL_FILE/WHITE-SM.PDF.

[30] C.W. Park, S.K. Kang, H.L. Hernandez, J.A. Kaitz, D.S. Wie, J. Shin, O.P. Lee, N.R. Sottos, J.S. Moore, J.A. Rogers, S.R. White, Thermally triggered degradation of transient electronic devices, Adv Mater. 27 (2015) 3783–3788. https://doi.org/10.1002/ADMA.201501180.

[31] R. Yoshida, T. Takahashi, T. Yamaguchi, H. Ichijo, Self-Oscillating Gel, Undefined. 118 (1996) 5134–5135. https://doi.org/10.1021/JA9602511.

[32] S. Maeda, Y. Hara, T. Sakai, R. Yoshida, S. Hashimoto, Self-Walking Gel, Advanced Materials. 19 (2007) 3480–3484. https://doi.org/10.1002/ADMA.200700625.

[33] R. Yoshida, Y. Murase, Self-oscillating surface of gel for autonomous mass transport, Colloids and Surfaces B: Biointerfaces. 99 (2012) 60–66. https://doi.org/10.1016/J.COLSURFB.2011.09.036.

[34] D. Suzuki, T. Kobayashi, R. Yoshida, T. Hirai, Soft actuators of organized self-oscillating microgels, Soft Matter. 8 (2012) 11447–11449. https://doi.org/10.1039/C2SM26477C.

[35] T. Sakata, S. Nishitani, Y. Yasuoka, S. Himori, K. Homma, T. Masuda, A.M. Akimoto, K. Sawada, R. Yoshida, Self-oscillating Chemoelectrical Interface of Solution-gated Ion-sensitive Field-effect Transistor Based on Belousov–zhabotinsky Reaction, Null. (2021). https://doi.org/10.21203/rs.3.rs-1110032/v1.

[36] T. Yamamoto, R. Yoshida, Self-oscillation of polymer and photo-regulation by introducing photochromic site to induce LCST changes, Reactive and Functional Polymers. 73 (2013) 945–950. https://doi.org/10.1016/J.REACTFUNCTPOLYM.2013.02.015.

[37] K. Homma, Y. Ohta, K. Minami, G. Yoshikawa, K. Nagase, A.M. Akimoto, R. Yoshida, Autonomous Nanoscale Chemomechanical Oscillation on the Self-Oscillating Polymer Brush

653 Surface by Precise Control of Graft Density., Langmuir. (2021).
654 https://doi.org/10.1021/acs.langmuir.1c00459.

655 [38] T. Geher-Herczegh, Z. Wang, T. Masuda, R. Yoshida, N. Vasudevan, Y. Hayashi, Delayed
656 Mechanical Response to Chemical Kinetics in Self-Oscillating Hydrogels Driven by the
657 Belousov-Zhabotinsky Reaction., Macromolecules. (2021).
658 https://doi.org/10.1021/acs.macromol.1c00402.

659 [39] M. Benoit, D. Bouyer, P. Sistat, A. Ayral, D. Cot, B. Rebiere, D. Fournier, J. Lyskawa, P. Woisel,
660 C. Antonelli, D. Quemener, Self-Oscillating Membranes with Polymer Interface Synchronized
661 with Chemical Oscillator to Reproduce Lifelike Pulsatile Flow, Chemistry of Materials. 33
662 (2021) 998–1005. https://doi.org/10.1021/acs.chemmater.0c04009.

663 [40] M.R. Whittaker, Y.K. Goh, H. Gemici, T.M. Legge, S. Perrier, M.J. Monteiro, Synthesis of
664 Monocyclic and Linear Polystyrene Using the Reversible Coupling/Cleavage of Thiol/Disulfide
665 Groups, Macromolecules. 39 (2006) 9028–9034. https://doi.org/10.1021/MA061070E.

666 [41] E. Cazares-Cortes, B.C. Baker, K. Nishimori, M. Ouchi, F. Tournilhac, Polymethacrylic Acid
667 Shows Thermoresponsivity in an Organic Solvent, Macromolecules. 52 (2019) 5995–6004.
668 https://doi.org/10.1021/acs.macromol.9b00412.

669 [42] I. Lacík, M. Stach, P. Kasák, V. Semak, L. Uhelská, A. Chovancová, G. Reinhold, P. Kilz, G.
670 Delaittre, B. Charleux, I. Chaduc, F. D'Agosto, M. Lansalot, M. Gaborieau, P. Castignolles, R.G.
671 Gilbert, Z. Szablan, C. Barner-Kowollik, P. Hesse, M. Buback, SEC Analysis of Poly(Acrylic Acid)
672 and Poly(Methacrylic Acid), Macromolecular Chemistry and Physics. 216 (2015) 23–37.
673 https://doi.org/10.1002/MACP.201400339.

674 [43] H. Lee, S.M. Dellatore, W.M. Miller, P.B. Messersmith, Mussel-inspired surface chemistry for
675 multifunctional coatings, Science (1979). 318 (2007) 426–430.
676 https://doi.org/10.1126/SCIENCE.1147241/SUPPL_FILE/LEE.SOM.PDF.

677 [44] M. Gu, J. Zhang, X. Wang, H. Tao, L. Ge, Formation of poly(vinylidene fluoride) (PVDF)
678 membranes via thermally induced phase separation, Desalination. 192 (2006) 160–167.
679 https://doi.org/10.1016/J.DESAL.2005.10.015.

680 [45] Y. Chen, X. Feng, Y. Zhao, X. Zhao, X. Zhang, Mussel-Inspired Polydopamine Coating Enhances
681 the Intracutaneous Drug Delivery from Nanostructured Lipid Carriers Dependently on a
682 Follicular Pathway, Molecular Pharmaceutics. 17 (2020) 1215–1225.
683 https://doi.org/10.1021/ACS.MOLPHARMACEUT.9B01240/SUPPL_FILE/MP9B01240_SI_001.P
684 DF.

685 [46] H. Sadegh, R. Sahay, S. Soni, Protein–polymer interaction: Transfer loading at interfacial
686 region of PES-based membrane and BSA, Undefined. 136 (2019).
687 https://doi.org/10.1002/APP.47931.

688 [47] F. Schacher, M. Ulbricht, A.H.E. Müller, Self-Supporting, Double Stimuli-Responsive Porous
689 Membranes From Polystyrene-block-poly(N,N-dimethylaminoethyl methacrylate) Diblock
690 Copolymers, Advanced Functional Materials. 19 (2009) 1040–1045.

691 [48] R.I. Peinador, J.I. Calvo, K. ToVinh, V. Thom, P. Prádanos, A. Hernández, Liquid-liquid
692 displacement porosimetry for the characterization of virus retentive membranes,
693 Journal of Membrane Science. 372 (2011) 366–372.
694 https://doi.org/10.1016/J.MEMSCI.2011.02.022.

Graphical Abstract